Morphological and mechanical properties of ultrahigh-molecular-weight polyethylene/low-molecular-weight polyethylene blend films produced by gelation/crystallization from solutions

Chie Sawatari
Faculty of Education, Shizuoka University, Shizuoka 422, Japan

and Masaru Matsuo*
Department of Clothing Science, Faculty of Home Economics, Nara Women's University, Nara 630, Japan
(Received 22 November 1988; accepted 24 January 1989)

Polyethylene–polyethylene blend films were prepared by gelation/crystallization from semidilute solutions by using ultrahigh-molecular-weight polyethylene (UHMWPE) ($M_w = 6 \times 10^6$) and low-molecular-weight polyethylene (LMWPE) ($M_w = 4 \times 10^4$). The UHMWPE/LMWPE compositions chosen were 91/9, 67/33 and 50/50. Elongation was carried out in a hot oven at 115–130°C. Drawability was dependent upon the compositions. The maximum achievable draw ratios of the 50/50 and 67/33 blends were 200-fold, while that of the 91/9 blend was 300-fold. The storage modulus decreases with increasing LMWPE content, when the measurements were carried out using specimens with the same draw ratio. Such mechanical properties were discussed in terms of morphological aspects by using wide-angle X-ray diffraction, birefringence, differential scanning calorimetry and optical microscopy.

(Keywords: polyethylene–polyethylene blend film; gelation/crystallization; ultrahigh-molecular-weight polyethylene; low-molecular-weight polyethylene; maximum achievable draw ratio)

INTRODUCTION

It was found that for a sufficiently high molecular weight the maximum achievable draw ratio depends principally on the concentration of the solution from which the gel was made[1–5]. This phenomenon was attributed to a reduced number of entanglements per molecule in solution-cast/spun polymers in comparison to those obtained from the melt. The ultradrawing of single-crystal mats is also based on the same concept[6–8]. The viscosities of solution and melt states of ultrahigh-molecular-weight polyethylene (UHMWPE) are far higher than those of low-molecular-weight polyethylene (LMWPE). Recent investigations of high-modulus fibre using LMWPE have been developed by Ward *et al.*[9,10] and Porter *et al.*[11,12].

It is certain that LMWPE still cannot produce fibres whose Young's modulus is higher than 100 GPa but it can produce fibres with Young's modulus of about 70 GPa. Such fibres are very important commercially, since the production rate of high-modulus fibres from UHMWPE gels is far below that commercially necessary and the drawability of melt films prepared from UHMWPE is lower than those prepared from LMWPE because of entanglements.

This paper deals with ultradrawing of blend gel films of UHMWPE and LMWPE for the purpose of preparing high-modulus fibres with Young's modulus > 100 GPa, since the viscosity of the solution undergoes a drastic decrease with increasing content of LMWPE. Studies of polyethylene blends have previously been investigated by several authors[13–16]. Gedde *et al.* have studied the morphology and crystallization of binary mixtures of sharp fractions of linear LMWPE by differential scanning calorimetry (d.s.c.) and small-angle light scattering (SALS)[13,14]. They reported that when blend samples were crystallized under isothermal conditions over a wide temperature range (380–430 K), three types of superstructure have been observed: axialites, non-banded spherulites and banded spherulites, each with characteristic crystallization. Minkova *et al.* studied the melting and crystallization behaviour of blends of LMWPE and UHMWPE prepared in the melt state[15]. They pointed out that the segregated melting and crystallization temperatures of both components do not depend on the composition of the blend, and the extreme enthalpy dependence of the blend composition is explained in terms of the mutual influence exhibited by the compositions with respect to each other. This was thought to be due to the inner stresses in non-flowing UHMWPE characterized by many entangled tie molecules.

Blends of UHMWPE and LMWPE gels, however, have never been studied. Accordingly, in the present work

* To whom correspondence should be addressed

0032-3861/89/091603-12$03.00

our focus is on the ultradrawing of blend films produced by gelation/crystallization from semidilute solutions according to the method of Smith and Lemstra[2,3]. The deformation mechanism of gel films with various compositions is investigated in terms of morphological and mechanical aspects.

EXPERIMENTAL

The samples used in this experiment were UHMWPE (Hercules 1900/90189) with a viscosity-average molecular weight of 6×10^6 and LMWPE (Sumikathen G 201) with that of 4×10^4. The solvent was decalin. The UHMWPE–LMWPE compositions chosen were 91/9, 67/33 and 50/50. Decalin solutions were prepared by heating the well blended polymer–solvent mixture at 135°C for 40 min under nitrogen flow. The hot homogenized solution was quenched to room temperature by pouring it into an aluminium tray, thus generating a gel. The decalin was allowed to evaporate from the gel under ambient conditions. The resulting gel was vacuum-dried for 1 day to remove residual traces of decalin. The gels could form a film, as long as the above compositions were used.

The dry gel film was cut into strips of length 30 mm and width 10 mm. The strips were clamped in a manual stretching device in such a way that the length to be drawn was 10 mm. The specimens were placed in a hot oven at 115–130°C and immediately elongated manually to the desired draw ratio λ.

The density of the films was measured by pycnometry with chlorobenzene–toluene as the medium. Since the density was very dependent on the presence of residual solvent in the film, great care was taken to remove the solvent. Samples were cut into fragments and immersed in an excess of ethanol for 30 days and subsequently vacuum-dried for 1 day prior to measuring the density.

The thermal behaviour was estimated from the melting endotherm in differential scanning calorimetry (d.s.c.) curves. D.s.c. measurements were carried out with a Rigaku 8230B thermal analyser. Dried gels, each weighing 1 mg, were placed in standard aluminium sample pans. Samples were heated at a constant rate of $10°C\,min^{-1}$.

SALS patterns were obtained with a 15 mW He–Ne gas laser as a light source. Diffuse surfaces were avoided by sandwiching the specimen between microcoverglasses with a silicone immersion oil having a similar refractive index.

Optical micrographs were obtained with a Nikon optical polarizer (XTP-11).

The X-ray measurements were carried out with a 12 kW rotating-anode X-ray generator (Rigaku RDA-rA). Wide-angle X-ray diffraction (WAXD) patterns were obtained with a flat camera using Cu K_α radiation at 200 mA and 40 kV. The X-ray beam was monochromatized with a curved graphite monochromator. SAXS patterns were obtained with a flat-film camera. The exposure time was 50 h. SAXS intensity distribution in the meridional direction was detected with a position-sensitive proportional counter (PSPC). The measurement was carried out by point focus with a three-pinhole collimator system. The corrected intensity was obtained by subtracting the contribution of the background (corresponding to air scattering) from the total intensity. The counting interval exposure time was 4×10^5 s for both total intensity and air scattering.

The complex dynamic tensile modulus was measured at 10 Hz over the temperature range from −65 to 160°C by using a viscoelastic spectrometer (VES-F) obtained from Iwamoto Machine Co. Ltd. The length of the specimen between the jaws was 40 mm and the width was about 1.5 mm. During measurements, the film was subjected to a static tensile strain in order to place the sample in tension during the axial sinusoidal oscillation, which had a peak deformation of 0.075%. The complex dynamic modulus was measured by imposing a small dynamic strain to assure linear viscoelastic behaviour of the specimen. Before the measurements were made, the undrawn and drawn films were annealed for 1 h at 90°C.

RESULTS AND DISCUSSION

Table 1 presents the preparation condition of UHMWPE–LMWPE blend gel films. The UHMWPE–LMWPE compositions chosen in this experiment were 91/9, 67/33 and 50/50. The concentration of solution to prepare gels was determined in such a way that the reference concentration of UHMWPE was fixed to be 0.5 g/100 ml and the concentration of LMWPE was determined from the value of UHMWPE–LMWPE composition. Such conditions proved most suitable to prepare gels. The resultant gels were found to form a film with high drawability. According to our previous work[17], gels of LMWPE had no ability to form a film. Hence the film formability of the blend gels is probably due to the fact that UHMWPE plays an important role to assure a suitable level of entanglement between UHMWPE and LMWPE chains.

Figure 1 shows WAXD and SAXS patterns (end view) for the original films of 91/9 and 50/50 compositions. The profiles of these patterns are hardly affected by the compositions. The WAXD patterns indicate the preferential orientation of the *c* axes perpendicular to the film surface. The SAXS patterns show the meridional scattering having scattering maxima corresponding to a long period of about 115 Å. This indicates that the dried gel films are composed of crystal lamellae that are highly oriented with their large flat faces parallel to the film surface. Based on the four patterns, it may be concluded that within the lamellar crystals constituting the gel, the *c* axes are oriented perpendicular to the large flat faces.

In order to obtain more detailed information, SAXS intensity distributions were observed for the original (undrawn) blends and the individual homopolymers in the meridional direction by PSPC system. *Figure 2* shows the results, in which the compositions 100/0 means the UHMWPE gel film prepared from solution with 0.5 g/100 ml and the composition 0/100 means the LMWPE gels (not film) prepared from solution with 2 g/100 ml. The profiles of the intensity distribution show

Table 1 Preparation condition of UHMWPE–LMWPE blend gels

UHMWPE–LMWPE composition	Concentration of solution (g/100 ml)		
	UHMWPE	LMWPE	Total
91/9	0.5	0.05	0.55
67/33	0.5	0.25	0.75
50/50	0.5	0.5	1.0

that the scattering maxima become more indistinct as the LMWPE content increases. This results is in good agreement with the previous result that the scattered maxima from the gels became indistinct as molecular weight decreased[17]. This result presumably indicates that LMWPE has no ability to form large lamellae that can become highly oriented with their large flat faces parallel to the film surface, when the gels are dried by slow evaporation of the solvent.

Figure 3 shows the change in the profiles of d.s.c. curves with different UHMWPE–LMWPE compositions. The curves have two peaks. The peaks on higher- and lower-temperature sides are associated with melting points of UHMWPE and LMWPE crystallites, respectively. The peak position due to the UHMWPE crystallites shifts to higher temperature with increasing content of UHMWPE, while the peak position due to LMWPE crystallites shifts to lower temperature.

Table 2 presents heats of fusion and crystallinities associated with UHMWPE and LMWPE crystallites for each specimen. Each heat of fusion was calculated by the relationship: heat of fusion = observed value/content of UHMWPE (or LMWPE). The crystallinity was calculated by assuming the heat of fusion of fully crystalline polymer[18] to be 286.8 kJ g^{-1}. The values are independent of the UHMWPE–LMWPE composition. This indicates that UHMWPE and LMWPE chains are crystallized independently by gelation from solution.

Figure 4 shows the change in the profile of the d.s.c. curves with increasing draw ratio for the 91/9, 67/33 and 50/50 blends. To check the reproducibility of the profile, d.s.c. measurements about a given draw ratio were carried out several times. The peak due to LMWPE crystallites within the 91/9 and 67/33 blends disappears and the peak for the 50/50 blend becomes extremely small. Such behaviour suggests two possibilities of oriented crystallization. One is growth of LMWPE crystallites and/or a decrease in the number of defects with crystallites which cause a peak shift to higher temperature corresponding to the peak position associated with the melting point of UHMWPE crystallites. The other is co-crystallization in such a way

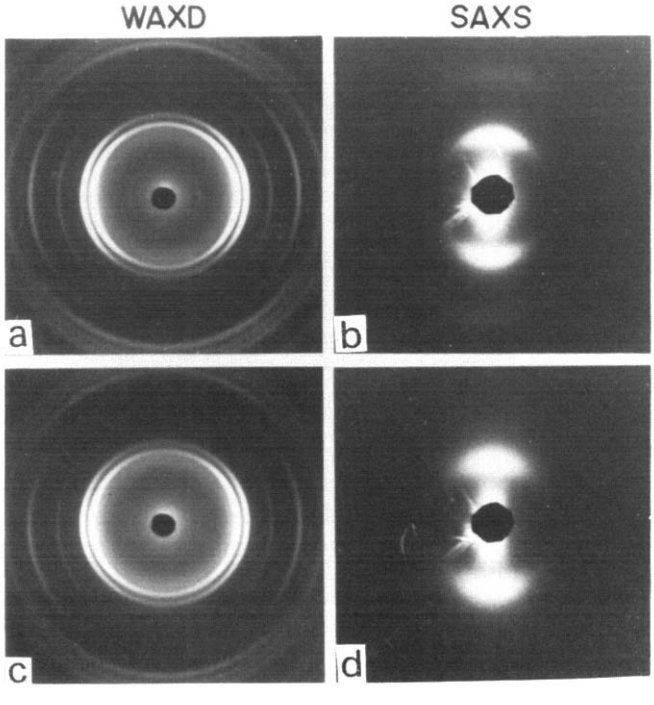

Figure 1 WAXD and SAXS patterns (end view) of the undrawn blend films. (a) and (b) 91/9 blend. (c) and (d) 50/50 blend

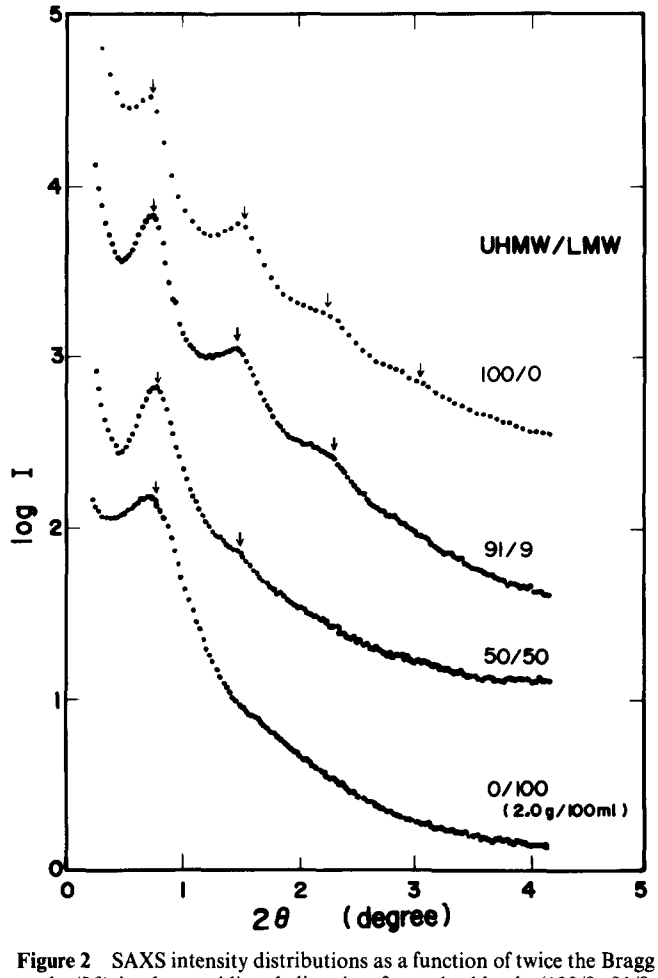

Figure 2 SAXS intensity distributions as a function of twice the Bragg angle (2θ) in the meridional direction from the blends (100/0, 91/9, 50/50 and 0/100)

Table 2 Heat of fusion (ΔH_u) and crystallinity of the blend films and the individual homopolymers

UHMWPE–LMWPE composition	UHMWPE		LMWPE	
	$-\Delta H_u$ (kJ g^{-1})	Crystallinity (%)	$-\Delta H_u$ (kJ g^{-1})	Crystallinity (%)
100/0	261.3	91.1	—	—
91/9	257.9	89.9	116.8	40.7
67/33	263.3	91.4	111.4	38.8
50/50	261.1	91.2	113.5	39.6
0/100	—	—	109.7	38.2

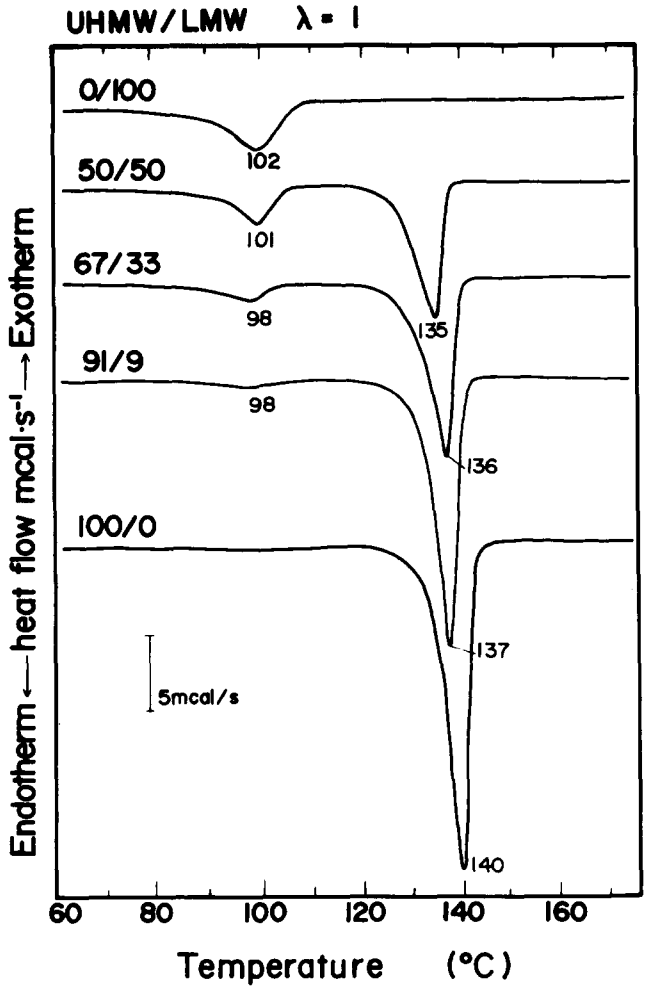

Figure 3 D.s.c. curves of the undrawn blends (100/0, 91/9, 67/33, 50/50 and 0/100)

that most of the UHMWPE and LMWPE chains are crystallized together to form the same crystallites. This problem will be discussed later in relation to the WAXD results. Incidentally, it is seen that the shoulder appears at the high-temperature side of the large main peak for the blends drawn up to $\lambda = 100$. The temperatures are higher than the equilibrium melting point (145.5°C) reported by Flory and Vrij[19]. This phenomenon is well known as a superheating effect which has been observed for highly oriented UHMWPE[20,21]. Therefore the observed melting points are probably not the true equilibrium values. The observed abnormally high apparent melting temperatures may be explained by assuming that polymer chains in the melt state retain the extended-chain arrangement and therefore the entropy of fusion would obviously be smaller than the value calculated for random coils in the melt.

Figure 5 shows the change in crystallinity of the UHMWPE–LMWPE blend gel films with increasing draw ratio. The values were estimated from the density. For the undrawn films, the crystallinity becomes higher as the UHMWPE content increases. The value for the UHMWPE homopolymer, however, is lower than that estimated from heats of fusion as listed in *Table 2*. The crystallinity also increases with increasing draw ratio. The crystallinities of the 100/0 and 91/9 blend films with $\lambda = 200$ reached 95 and 94%, respectively, and those of the 67/33 and 50/50 blends reached about 84 and 81%, respectively. This indicates that the LMWPE with high degree of branching ($2.5\,CH_3/100\,C$) hampers the increase in crystallinity.

Figure 6 shows the change in birefringence with increasing draw ratio. The birefringences of the 91/9, 67/33 and 50/50 blend films reached 63×10^{-3}, 61×10^{-3} and 59.5×10^{-3}, respectively, at $\lambda = 200$, and these values are higher than the intrinsic birefringence of crystalline phase, 58.5×10^{-3}. This discrepancy is probably due to the fact that the value of crystalline birefringence may be incorrect and that form birefringence, which has been neglected, may be significant. The intrinsic birefringence of the crystalline phase is calculated from the three principal refractive indices of a crystal of the n-paraffin ($C_{36}H_{74}$) reported by Bunn and de Daubeny[22]. This calculation is based on the assumption that the principal refractive indices can be estimated by assuming the atomic arrangements within the crystal unit cell and neglecting the uncertain effects of the internal field. Furthermore, the form birefringence cannot be neglected because a number of voids were observed within the drawn specimens under scanning electron microscopy[23]. Unfortunately, there is no way at present to estimate the form birefringence. The birefringence data indicate that molecular chains within the three kinds of blend films drawn to $\lambda = 200$ show highly orientational degrees with respect to the stretching direction. The small difference of the birefringence values among the blends is probably due to the difference of the crystallinity as shown in *Figure 5* but is independent of the orientational degree of molecular chains.

In order to obtain more detailed information of molecular orientation, WAXD patterns were obtained. *Figure 7* shows the change in WAXD patterns from the three kinds of blends with increasing draw ratio λ. The patterns beyond $\lambda = 50$ exhibit a high degree of orientation of the c axes with respect to the stretching direction. This tendency is almost independent of the UHMWPE–LMWPE compositions. However, the reflections from the (110) and (200) planes indicate that at $\lambda = 20$ there exist two kinds of orientational modes for crystallites within the 67/33 and 50/50 blend films; one is a high degree of orientation of the c axes corresponding to the strong equatorial reflection spots and the other is an insufficient orientation corresponding to the large arcs. In contrast, the pattern of the 91/9 blend at $\lambda = 20$ shows strong equatorial spots, indicating a high degree of orientation of the c axes. Hence it may be expected that the orientational degree is pronounced with increasing content of UHMWPE. This tendency is in good agreement with the results in *Figure 5*. The strong spots are thought to be due to the reflection from UHMWPE crystallites, while the arcs are due to LMWPE ones.

In order to justify this concept, WAXD patterns were observed with increasing temperature. *Figure 8* shows the results for the 50/50 blend films at $\lambda = 20$, when the sample was fixed at a constant stress of 0.011 GPa to avoid shrinkage of the film. The specimens were annealed for 10 min at the indicated temperature prior to photographing. As can be seen in a series of patterns, the reflections from the (110) and (200) planes shift to smaller diffraction angles. The large arcs from the (110) plane disappeared at 150°C due to melting but the reflection spots remained. This result supports our assumption that the large arcs are due to the reflection from the LMWPE crystallites with poor preferential

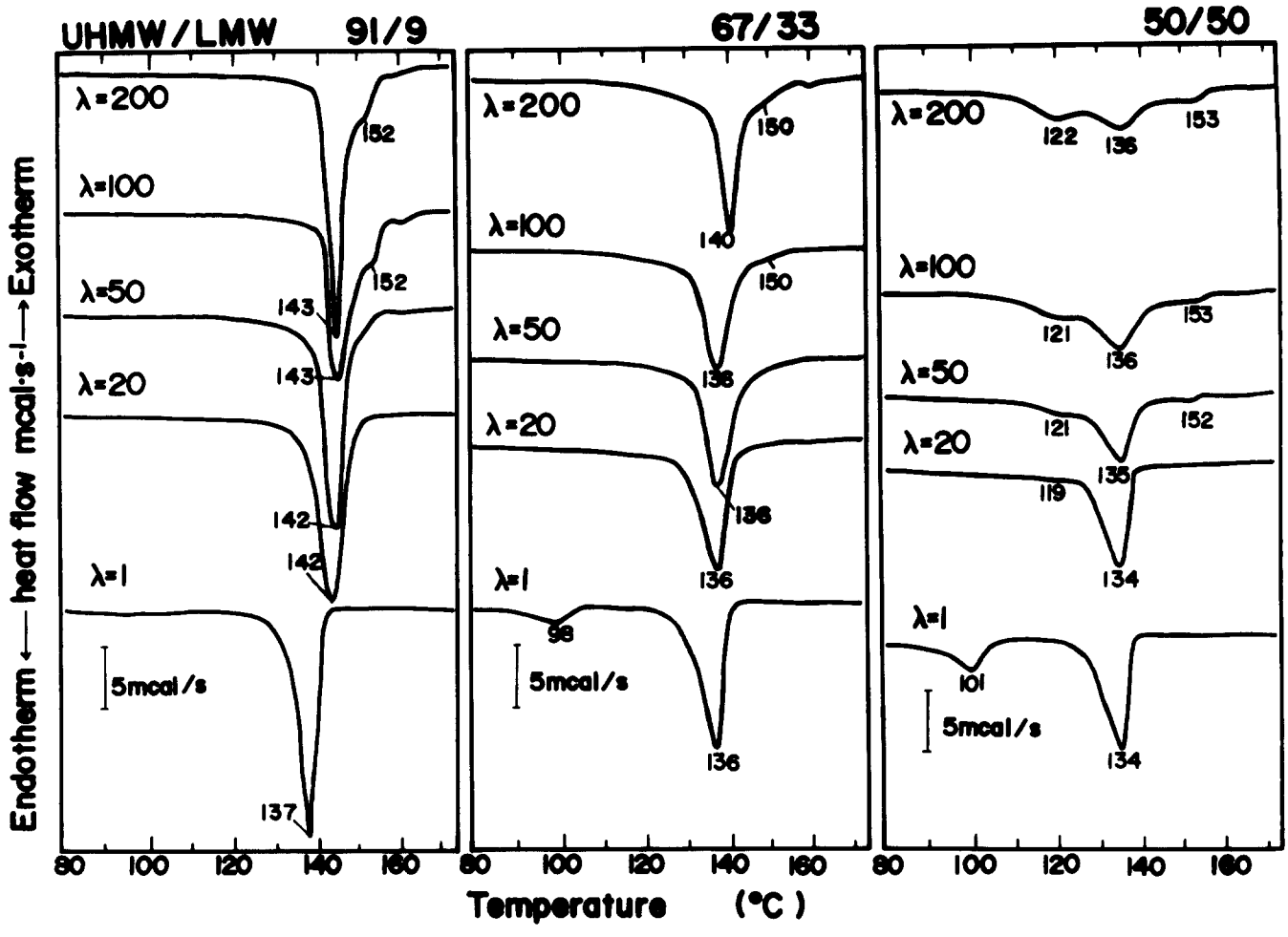

Figure 4 D.s.c. curves of the blends (91/9, 67/33 and 50/50) drawn to various draw ratios λ

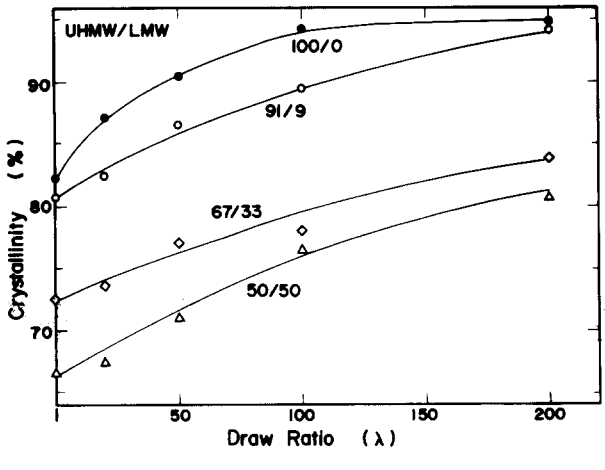

Figure 5 Change in crystallinity of the 100/0, 91/9, 67/33 and 50/50 blends against draw ratio λ

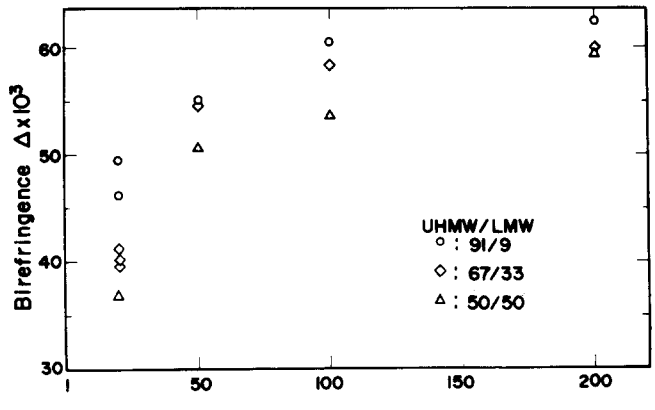

Figure 6 Change in birefringence of the 91/9, 67/33 and 50/50 blends against draw ratio λ

orientational degree with respect to the stretching direction, while the strong spots are due to the reflection from the UHMWPE crystallites with highly orientational degree. Such detailed information, however, cannot be obtained from the d.s.c. measurements. As can be seen in *Figure 4*, the profile of the 50/50 blend film with $\lambda=20$ shows a small peak around 119°C and a large peak around 134°C and these melting points are much lower than those obtained from X-ray diffraction measurements. This discrepancy is due to the differences of heating conduction mechanism and of sample setting. In the d.s.c. measurement, heating of the sample was carried out without any constraint through the aluminium sample pan, while in the X-ray measurements, the heating was carried out with dimensions fixed under hot air in an oven.

Figure 9 shows the WAXD patterns for the 50/50 blend film with $\lambda=200$ at 20 and 150°C. The strong spots are due to the reflections from both UHMWPE and LMWPE crystallites. The spots remained at 150°C but the intensity at 150°C becomes a little weaker than those

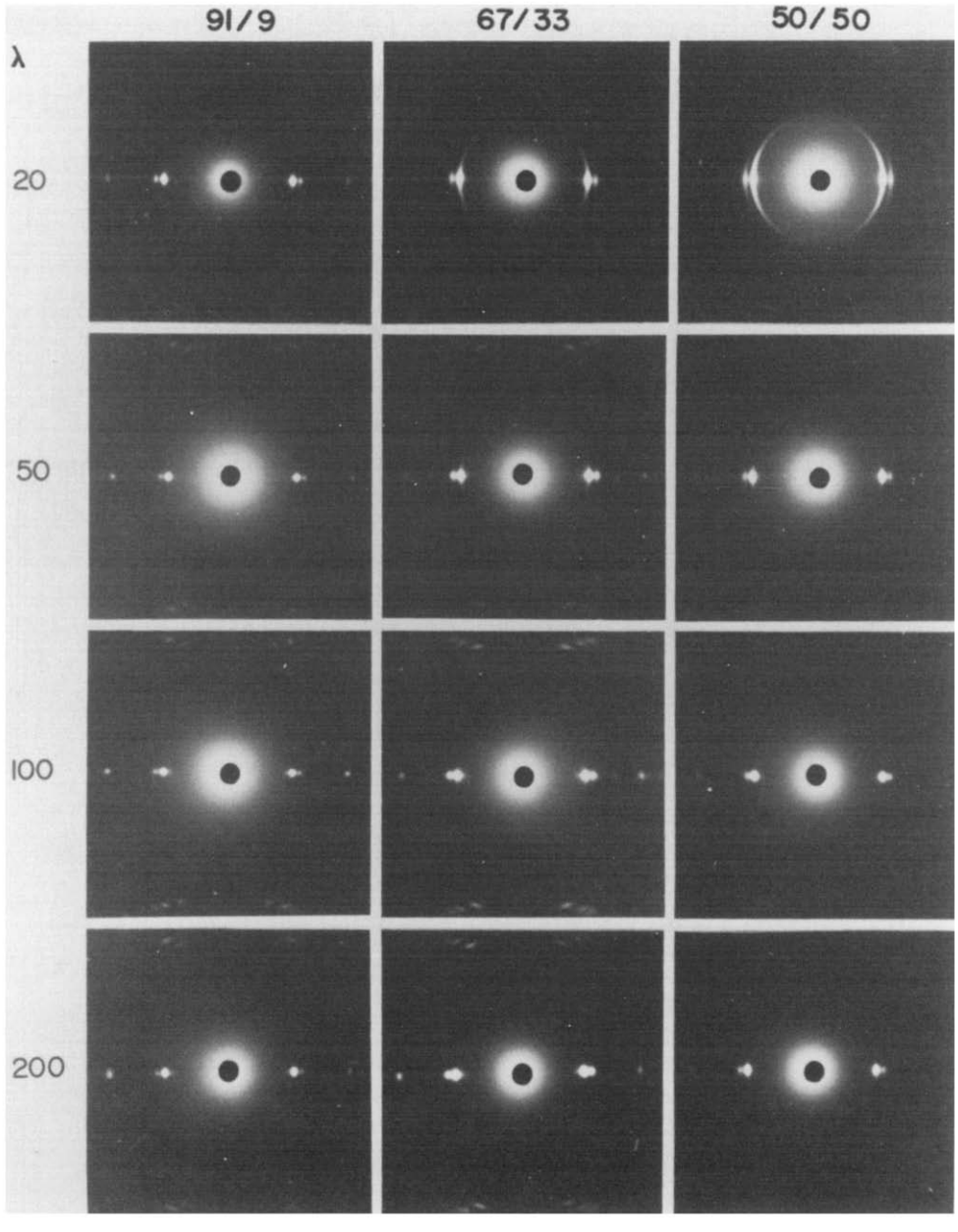

Figure 7 WAXD patterns (through view) from the 91/9, 67/33 and 50/50 blends at various draw ratios λ

at 20°C. This indicates that, although the orientational fluctuation of crystallites is hardly affected by temperatures up to 150°C, the partial melting of crystallites has arisen. The reflection spots from UHMWPE crystallites at 150°C are due to the superheating phenomenon associated with extended-chain crystallites whose apparent melting point from the d.s.c. measurements was 153°C, as shown in *Figure 4*.

In order to estimate the above results quantitatively, the total diffraction intensity from the (110) and (200) planes in the meridional direction were observed as a function of temperature for the 100/0, 91/9 and 50/50 blends with $\lambda=200$. The intensity I was measured at a step interval of 0.1° with a time of 10 s in the range 14 to 32° (twice the Bragg angle 2θ) and was represented as a function of Is^2 *versus* s ($s=2\sin\theta/\lambda$, λ being the wavelength of the X-rays). All intensities at the indicated temperatures were normalized by that at 20°C, which is given by:

$$\text{Normalized value}=\frac{\int_{s_1}^{s_2} I(T,s)s^2\,ds}{\int_{s_1}^{s_2} I(T=20°,s)s^2\,ds}$$

where s_1 and s_2 correspond to $s(=2\sin\theta/\lambda)$ at $\theta=7$ and 16°, respectively.

Figure 10 shows the result. The values show a gradual decrease with temperature and this tendency becomes more pronounced as the LMWPE content increases. A drastic decrease around 150°C is due to the melting of LMWPE crystallites.

Figure 11 shows the change in birefringence with increasing temperatures, observed for the three kinds of blends with $\lambda=20$. The birefringence data of the 50/50 blend are independent of temperatures $<90°$ but they

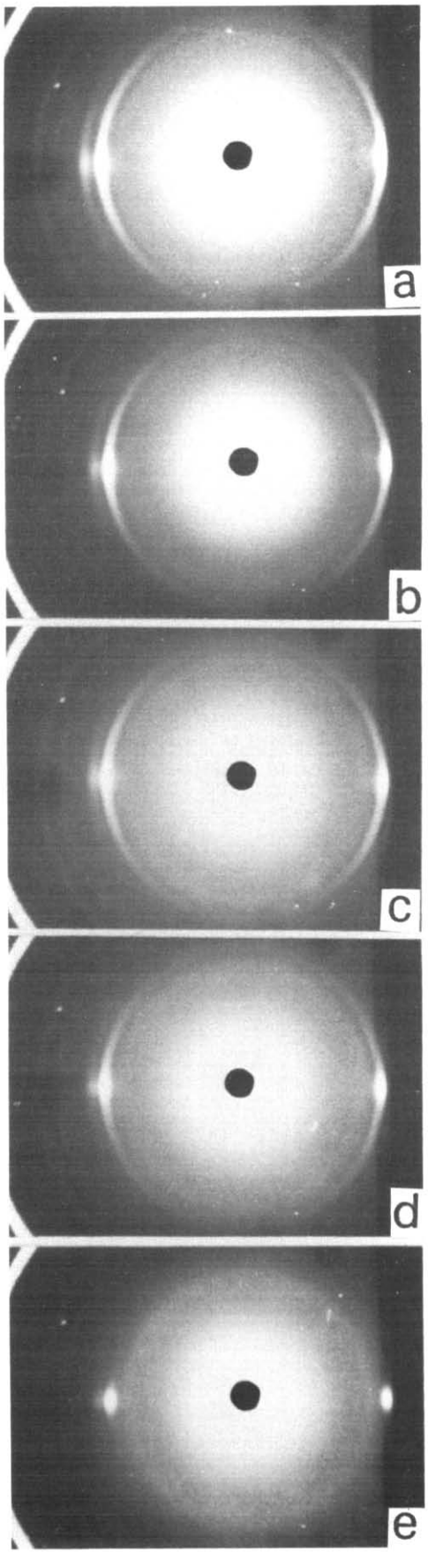

Figure 8 Change in WAXD patterns (through view) from the 50/50 blend film ($\lambda = 20$) at various temperatures. (a) 20°C; (b) 100°C; (c) 130°C; (d) 140°C; (e) 150°C

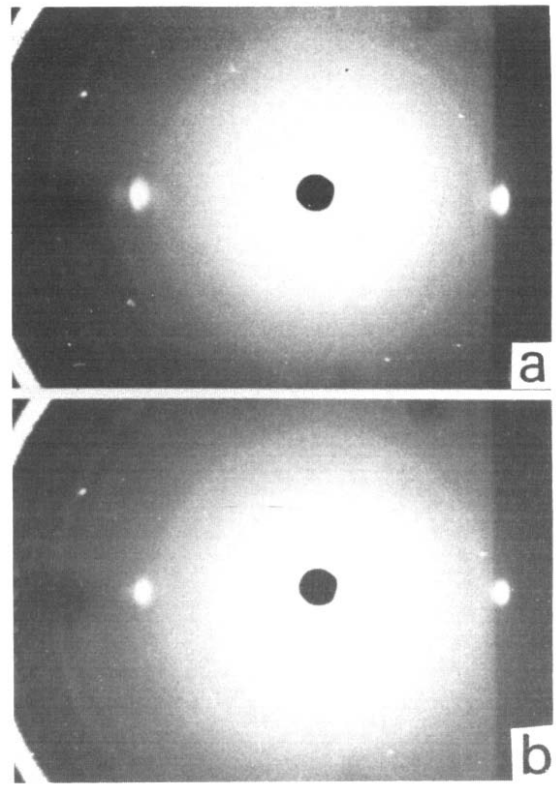

Figure 9 WAXD patterns (through view) from the 50/50 blend film ($\lambda = 200$) at (a) 20°C and (b) 150°C

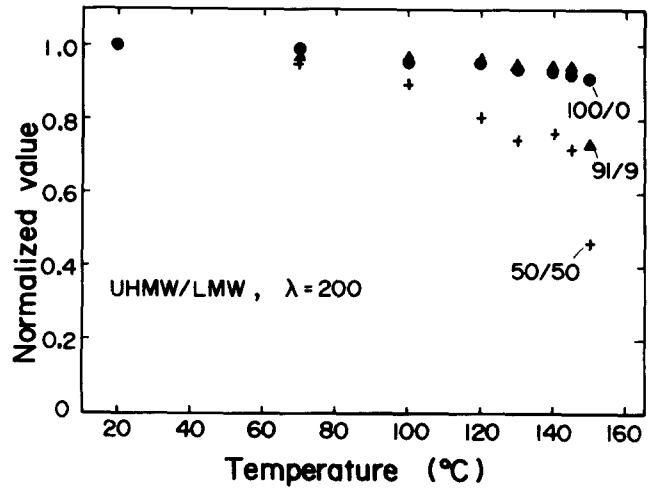

Figure 10 The normalized total X-ray diffraction intensity as a function of temperature

decreased with further increase of temperature. In contrast, the temperature dependence of the molecular orientation cannot be observed from birefringence data for the 91/9 and 67/33 blends. This result supports the WAXD patterns in *Figure 7* in which the strong equatorial spots due to UHMWPE crystallites remained up to 150°C, while the arcs due to LMWPE crystallites disappeared due to melting. The orientational fluctuation of chain segments by melting of crystallites, however, can be detected by the birefringence data only for the 50/50 blend, but, as a whole, birefringence is not sensitive enough to detect small changes in the molecular orientation within specimens like 91/9 and 67/33 blends.

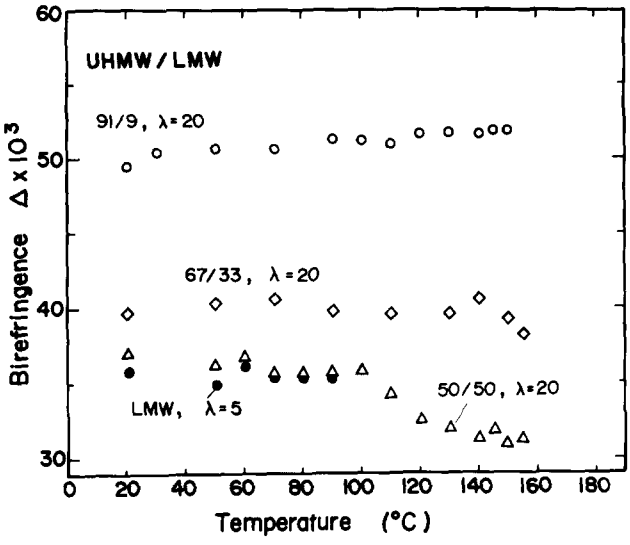

Figure 11 Change in birefringence of the 91/9, 67/33 and 50/50 blends ($\lambda = 20$) with increasing temperature

Figure 12 shows H_v light scattering patterns from the three kinds of blends as a function of draw ratio. Patterns of the undrawn 91/9 and 67/33 blend films display lobes of a diffuse X-type. The intensity had a maximum in the scattering centre and decreased monotonically with increasing scattering angle. These observations are indicative of scattering from rodlike textures. The existence of rodlike texture has already been observed for UHMWPE dried gel films[24]. As for a pattern of the 50/50 blend film, the notch of the lobes is clear, especially in the scattering centre region. However, it is very difficult to discern the position of scattering maxima in the lobes. According to the previous paper[17], it turned out that the dry gels of LMWPE are constructed from spherulitic textures. Based on this fact, such a pattern is thought to be due to the scattering from both rodlike and spherulitic textures.

Elongation up to $\lambda = 20$ causes development of the X-type pattern with maximum intensity at odd multiples of 45° with respect to the equatorial direction for three blend films. Furthermore, the intensity becomes a

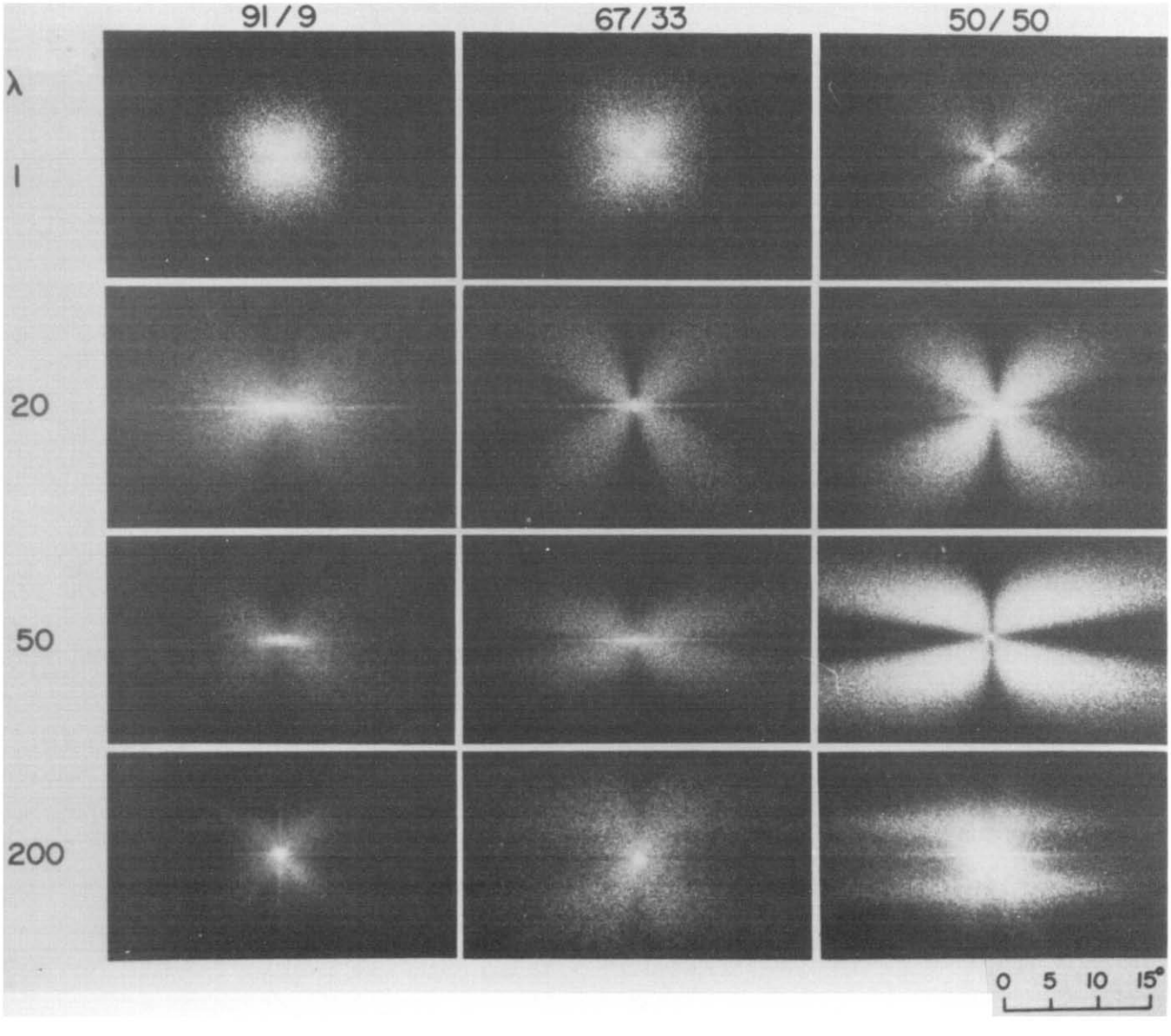

Figure 12 Change in H_v light scattering patterns from the 91/9, 67/33 and 50/50 blend films at various draw ratios λ

maximum at a scattering centre for each lobe. Such patterns are indicative of scattering from rodlike textures, which have been observed for undrawn films[25]. As shown in *Figures 5* and 7, however, the molecular chains within the three kinds of blend take preferential orientation with respect to the stretching direction. This indicates that the rods within the blends orient at $\pm 45°$ with respect to the stretching direction and the molecular chain axes corresponding to the optical axes orient predominantly in the stretching direction. Such interesting patterns have been observed in the oriented crystallization process of polyethylene callendered film[25] and poly(butylene terephthalate)[26,27]. Scattering from deformed spherulites cannot be discerned within the 50/50 blend. Therefore it may be confirmed that the possibility of the existence of rodlike textures within the 50/50 blend is higher than that of spherulitic ones.

On increasing λ beyond 50, the scattering lobes are extended in the horizontal direction. Among these patterns, the patterns from the 91/9 and 67/33 blends indicate scattering from rods oriented predominantly in the stretching direction. In contrast, scattering from the 50/50 blend with $\lambda = 50$ displays a distinct four-leaf pattern whose lobes are extended in the horizontal direction, indicative of the existence of deformed spherulites. The pattern is quite similar to that from LMWPE melt film drawn to $\lambda = 5$ as shown in *Figure 13*. The disappearance of the scattering from rods is probably due to the destruction of rods and/or the almost perfect orientation of the optical axes within rods in the stretching direction. Furthermore, the patterns from the three kinds of blends with $\lambda = 200$ are indistinct, indicating scattering from complicated structures that have arisen by disruptive deformation of rods and/or spherulites. Such complicated changes of SALS patterns cannot be analysed on the basis of the results of WAXD patterns in *Figure 7* and of birefringence in *Figure 6*. The detailed analysis was carried out using optical microscopy under crossed polarizers.

In the optical microscope, the development of the fibrous texture could be readily followed. *Figure 14* shows the appearance of the specimen with stretching. At this scale of magnification, it is very difficult to recognize the difference of morphological features among the three kinds of blend films. At $\lambda = 20$, close observation reveals that the texture is composed of a stack of oriented lamellae. These units are oriented at a particular angle of $\pm 45°$ with respect to the stretching direction to form a network structure. This observation is in good agreement with the SALS patterns of the blend films with $\lambda = 20$ in *Figure 12*. For the 91/9 blend films, the width of rods decreases drastically beyond $\lambda = 20$ and finally the rods seem to be disruptively deformed into fine fibrils. The fibrils are also highly oriented parallel to the stretching direction. The photographs at $\lambda = 50$ and 100 are in good agreement with the corresponding SALS patterns in *Figure 12*. The photograph of the 50/50 blend film with $\lambda = 50$ exhibits the existence of complicated structures deformed in the stretching direction. The structures were thought to be deformed spherulites, based on the SALS pattern in *Figure 12*. The photographs of the blends with $\lambda = 200$ are too indistinct to discern the shape of superstructures to analyse the corresponding SALS patterns.

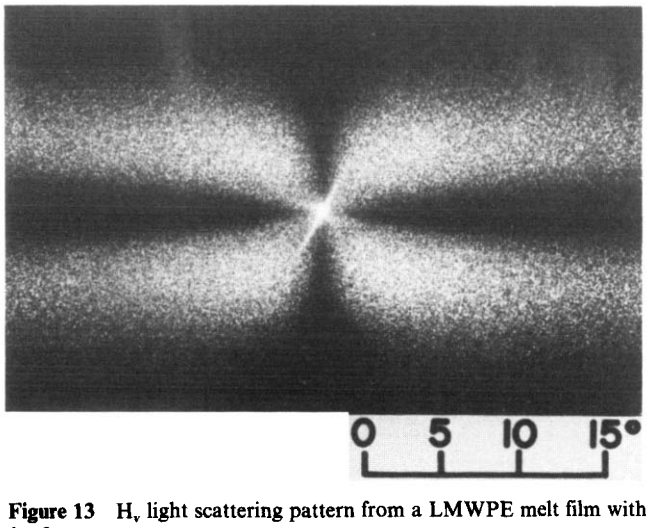

Figure 13 H_v light scattering pattern from a LMWPE melt film with $\lambda = 5$

Figure 15 shows the behaviour of the storage and loss moduli for the undrawn blend films. The storage modulus increases on increasing the UHMWPE content. This is probably due to an increase in crystallinity, as shown in *Figure 5*. The magnitude of the storage modulus increases as the temperature decreases, and this tendency is pronounced with increasing content of UHMWPE.

The loss modulus shows a large peak of the α mechanism around 80°C associated with crystal dispersion[28]. The β mechanism associated with amorphous dispersion cannot be observed for the three kinds of blend films. This is probably due to high crystallinity of the blend gel films used in this experiment. For example, even the crystallinity of the 50/50 blend is beyond 67%, which is higher than the crystallinity of the undrawn melt films[29].

Figures 16–18 show the temperature dependence of the storage and loss moduli for the blend gel films drawn to $\lambda = 20$, 50 and 200, respectively. As can be seen in a series of experimental results, the storage modulus becomes higher with increasing UHMWPE content and draw ratio, because of the increase in crystallinity and orientational degree of molecules as shown in *Figures 5* and *6*. As can be seen in *Figure 18*, the storage modulus at 20°C reached about 170 and 100 GPa for the UHMWPE homopolymer and the 50/50 blend film with $\lambda = 200$, respectively. The possibility of successfully drawing up to $\lambda = 200$ becomes lower as the UHMWPE content increases. The possibility for the 50/50 blend film was less than 10%. As can be seen in *Figure 17*, the storage modulus of the 50/50 blend film is beyond 60 GPa at 20°C and this value is about half of the value of the UHMWPE homopolymer. Interestingly, the viscosity of the solution with 50/50 blend at 135°C was found to be much lower than that with UHMWPE homopolymer in the same concentration regime. As discussed before, the Young's modulus (corresponding to the storage modulus) of 50 GPa is enough for the usual applications, except special-purpose ones. Hence it may be expected that the UHMWPE–LMWPE blend films with low content of LMWPE such as 50/50 blend will play an important role in terms of the production rate at commercially interesting speed because of the drastic decrease in the viscosity in the melt state and/or solution.

The loss modulus has a large peak around 80°C associated with the α mechanism for all the specimens at $\lambda = 20$. With further elongation, the loss modulus has

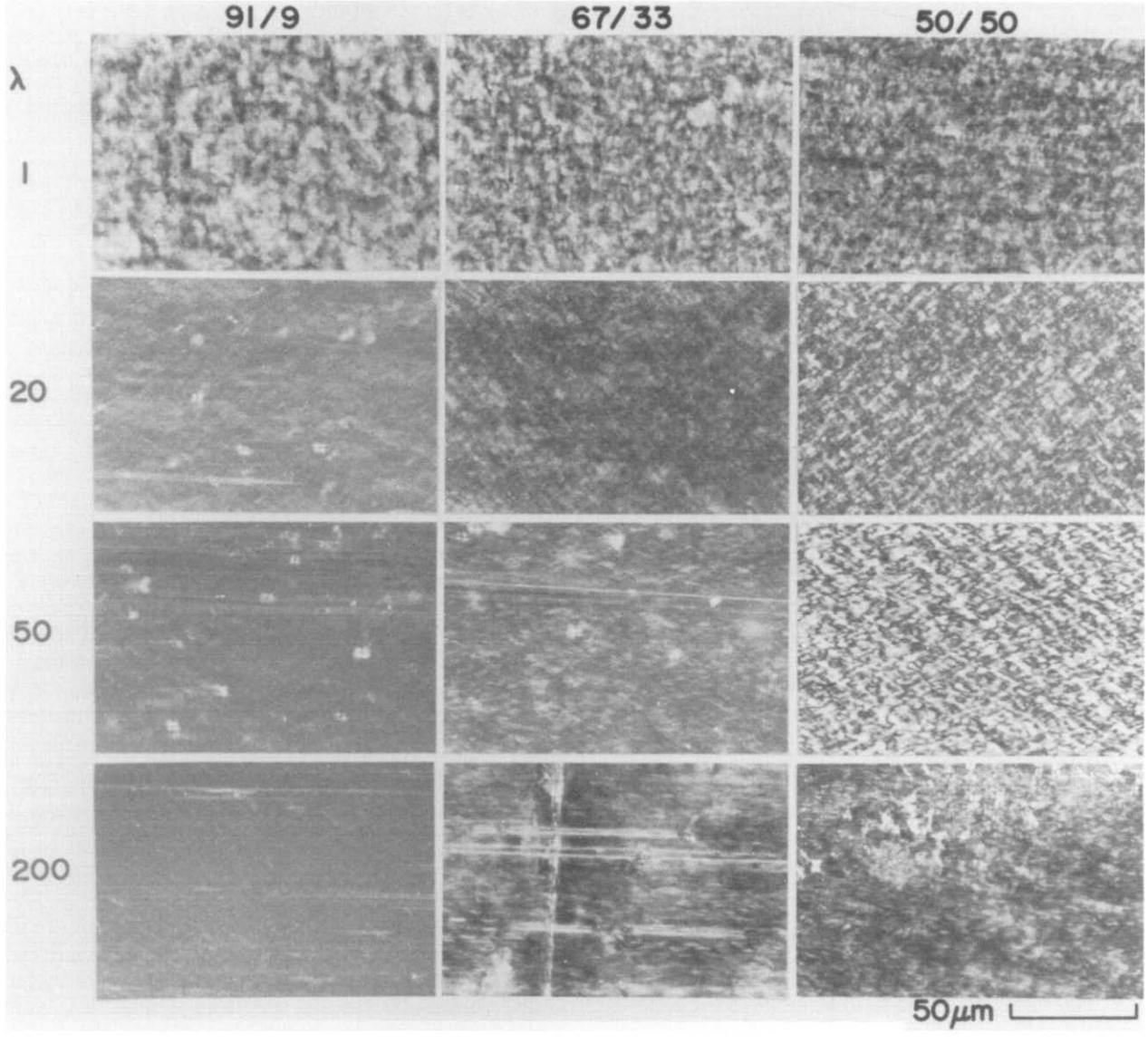

Figure 14 Optical micrographs (crossed polarizers) of the 91/9, 67/33 and 50/50 blend films at various draw ratios λ. In the 91/9 blend ($\lambda = 20$) and 67/33 blends ($\lambda = 50$ and 200) the white lines along the stretching direction (horizontal direction) are cracks

another peak at a temperature beyond 110°C in addition to the α mechanism peak but the magnitude of this peak becomes pronounced with increasing content of LMWPE. Such a peak, however, cannot be observed for the UHMWPE homopolymer. Accordingly, the appearance of this peak is associated with an increase in viscosity due to melting of LMWPE crystallites within the blend films.

Incidentally, the storage modulus at $\lambda = 300$ for the 91/9 blend reached 165 GPa at 20°C. This value is less than 200 GPa of the UHMWPE homopolymer at $\lambda = 300$[23] because of low crystallinity and/or defects within crystallites of LMWPE.

CONCLUSIONS

Ultrahigh-molecular-weight polyethylene (UHMWPE)/low-molecular-weight polyethylene (LMWPE) blend films were prepared by gelation/crystallization from semidilute solutions. The viscosity-average molecular weights of UHMWPE and LMWPE were 6×10^6 and 4×10^4, respectively. The UHMWPE–LMWPE compositions chosen were 91/9, 67/33 and 50/50. For all compositions a concentration of UHMWPE of 0.5 g/100 ml proved most suitable to prepare the gels. The resultant blend films after evaporating the solvent could be readily elongated to a desired draw ratio in a hot oven at 130°C. The morphological and mechanical properties of the blend films were dependent upon the compositions.

D.s.c. curves of the undrawn blend films show two peaks corresponding to the individual homopolymers. The peak due to UHMWPE crystallites appeared around 135–140°C and those due to LMWPE crystallites around 98–101°C. When the films were stretched beyond $\lambda = 20$, the peak due to the LMWPE crystallites disappeared, since the peak shifted to higher temperatures corresponding to the peak associated with the melting of the UHMWPE crystallites. This indicated a decrease in the number of defects within LMWPE crystallites by oriented crystallization.

The orientational mode of crystallites is sensitive to composition at draw ratios lower than 20. The orientational degree of the LMWPE crystallites becomes poorer as the LMWPE content increases. Beyond $\lambda = 50$,

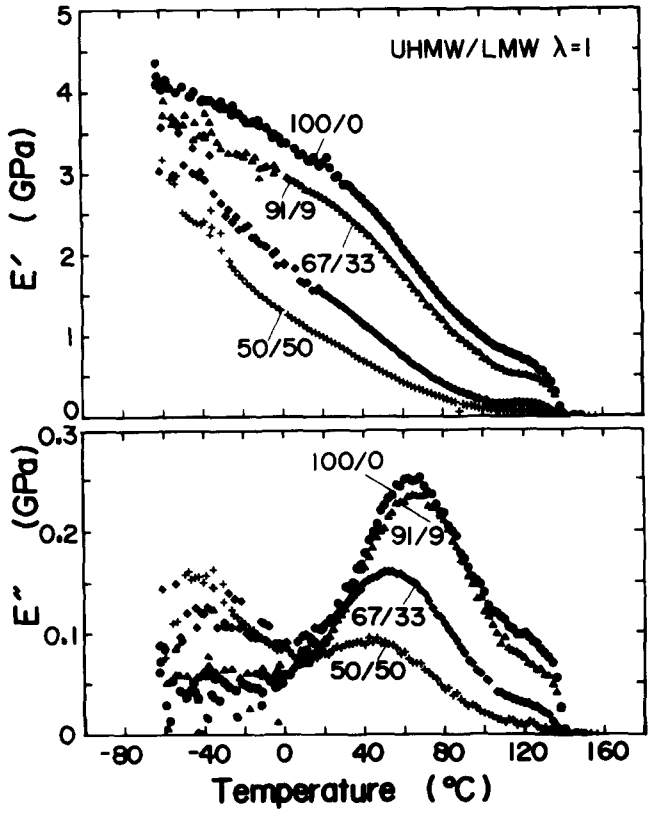

Figure 15 Temperature dependence of the storage and loss moduli for the 100/0, 91/9, 67/33 and 50/50 blends in an undrawn state

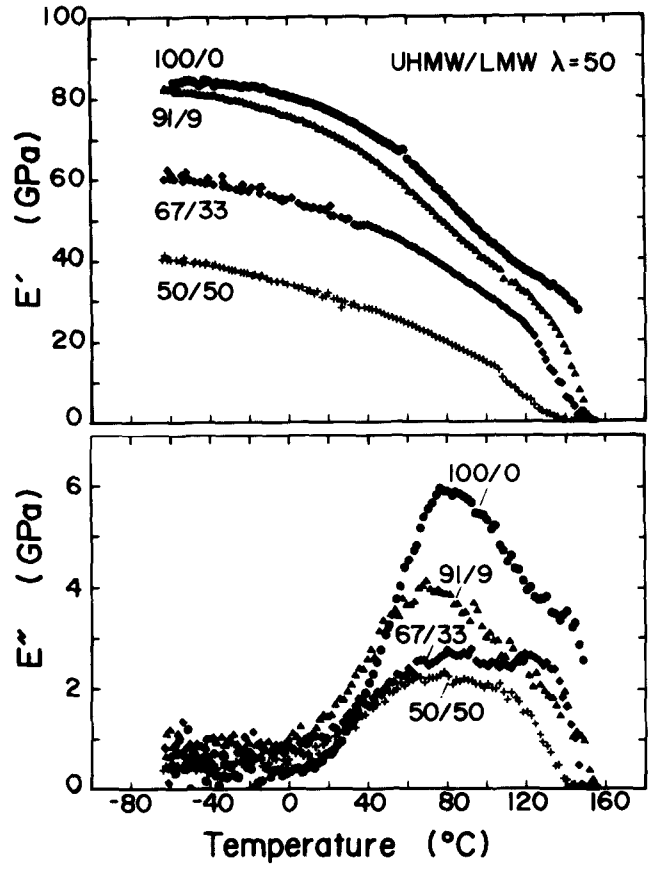

Figure 17 Temperature dependence of the storage and loss moduli for the 100/0, 91/9, 67/33 and 50/50 blends ($\lambda = 50$)

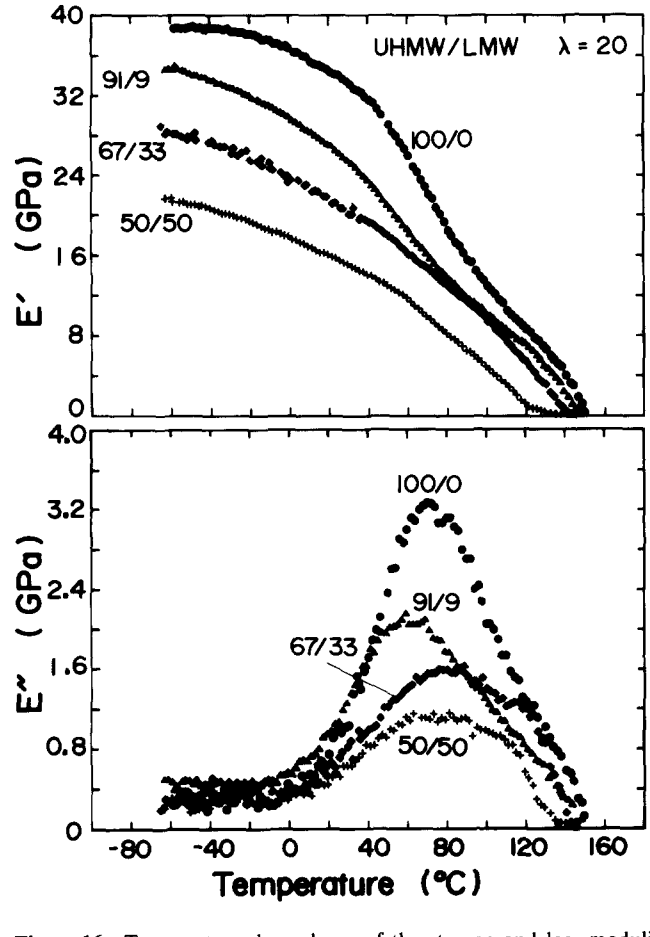

Figure 16 Temperature dependence of the storage and loss moduli for the 100/0, 91/9, 67/33 and 50/50 blends ($\lambda = 20$)

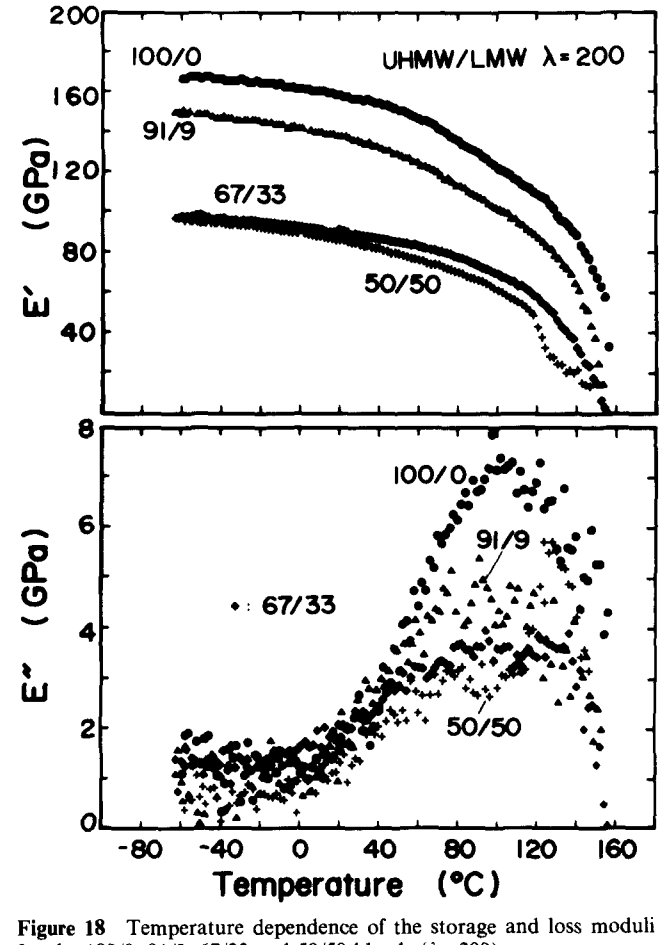

Figure 18 Temperature dependence of the storage and loss moduli for the 100/0, 91/9, 67/33 and 50/50 blends ($\lambda = 200$)

however, the LMWPE crystallites took the extremely high orientation like UHMWPE crystallites. Such orientational behaviour of the LMWPE crystallites is probably due to the existence of a suitable level of entanglement between UHMWPE and LMWPE chains. Namely, following taut tie molecules due to the orientation of UHMWPE crystallites, the LMWPE crystallites cause a significant transformation from a folded to a fibrous type.

The storage modulus of the blend films decreases when the LMWPE content increases. The storage modulus of the 50/50 blend film with $\lambda = 200$, however, remained about 60 GPa at 20°C, and this value is enough for the usual applications of polyethylene fibres under ambient conditions.

ACKNOWLEDGEMENT

We thank Dr T. Asano, Department of Physics, Shizuoka University, for his kind help in obtaining the d.s.c. curves.

REFERENCES

1 Smith, P., Lemstra, P. J., Kalb, B. and Pennings, A. J. *Polym. Bull.* 1979, **1**, 733
2 Smith, P. and Lemstra, P. J. *J. Mater. Sci.* 1980, **15**, 505
3 Smith, P., Lemstra, P. J. and Booij, H. C. *J. Polym. Sci., Polym. Phys. Edn.* 1981, **19**, 877
4 Matsuo, M., Sawatari, C., Iida, M. and Yoneda, M. *Polym. J.* 1985, **17**, 1197
5 Matsuo, M. and Sawatari, C. *Macromolecules* 1986, **19**, 2036
6 Kanamoto, T., Tsuruta, A., Tanaka, K., Takeda, M. and Porter, R. S. *Polym. J.* 1983, **15**, 327
7 Furuhata, K., Yokokawa, T. and Miyasaka, K. *J. Polym. Sci., Polym. Phys. Edn.* 1984, **22**, 133
8 Kanamoto, T., Tsuruta, A., Tanaka, K., Takeda, M. and Porter, R. S. *Macromolecules* 1988, **21**, 470
9 Andrews, J. M. and Ward, I. M. *J. Mater. Sci.* 1970, **5**, 411
10 Clements, J., Capaccio, G. and Ward, I. M. *J. Polym. Sci., Polym. Phys. Edn.* 1979, **17**, 693
11 Zachariades, A. E., Mead, W. T. and Porter, R. S. in 'Ultra-high Modulus Polymers' (Eds. A. Ciferri and I. M. Ward), Applied Science, London, Ch. 2, p. 77
12 Kojima, S. and Porter, R. S. *J. Polym. Sci., Polym. Phys. Edn.* 1978, **16**, 1729
13 Lopez, J. M. R. and Gedde, U. W. *Polymer* 1988, **29**, 1037
14 Lopez, J. M., Brana, M. T. C., Terselius, B. and Gedde, U. W. *Polymer* 1988, **29**, 1045
15 Minkova, L. and Mihailov, M. *Colloid Polym. Sci.* 1987, **265**, 1
16 Minkova, L. *Colloid Polym. Sci.* 1988, **266**, 6
17 Sawatari, C., Okumura, T. and Matsuo, M. *Polym. J.* 1986, **18**, 741
18 Mandelkern, L. *Rubber Chem. Technol.* 1959, **32**, 1392
19 Flory, P. J. and Vrij, A. J. *J. Am. Chem. Soc.* 1963, **85**, 3548
20 Matsuo, M. and Manley, R. S. J. *Macromolecules* 1983, **16**, 1500
21 Sawatari, C. and Matsuo, M. *Colloid Polym. Sci.* 1985, **263**, 783
22 Bunn, C. W. and de Daubeny, R. *Trans. Faraday Soc.* 1954, **50**, 1173
23 Matsuo, M., Inoue, N. and Abumiya, N. *Sen-i-Gakkaishi* 19XX, **40**, 275
24 Matsuo, M. and Manley, R. S. J. *Macromolecules* 1982, **15**, 985
25 Kang, S. J. and Matsuo, M. *Polym. J.* in press
26 Sawatari, C., Muranaka, M. and Matsuo, M. *Polym. J.* 1983, **15**, 33
27 Sawatari, C., Iida, M. and Matsuo, M. *Macromolecules* 1984, **17**, 1765
28 Raff, R. A. V. in 'Encyclopedia of Polymer Science and Technology' (Eds. H. F. Mark *et al.*), Wiley, New York, 1967, vol. 6, pp. 275–332
29 Matsuo, M. and Sawatari, C. *Macromolecules* 1988, **21**, 1317